Bioorganic Chemistry 86 (2019) 665–673

Contents lists available at ScienceDirect

Bioorganic Chemistry

journal homepage: www.elsevier.com/locate/bioorg

# Alkene lactones from *Persea fulva* (Lauraceae): Evaluation of their effects on tumor cell growth *in vitro* and molecular docking studies

Isabella Mary Alves Reis[a], Rodrigo Souza Conceição[a], Rafael Short Ferreira[b], Cleonice Creusa dos Santos[b], Girliane Regina da Silva[c], Larissa de Mattos Oliveira[a], Dayse Santos Almeida Cassiano[a], Manoelito Coelho dos Santos Junior[a], Mariana Borges Botura[a], Victor Diogenes Amaral da Silva[b], Silvia Lima Costa[b], Tania Maria Sarmento da Silva[c], Ivo José Curcino Vieira[d], Raimundo Braz-Filho[e,f], Alexsandro Branco[a,*]

[a] Departamento de Saúde, Universidade Estadual de Feira de Santana, Av. Transnordestina s/n, 44036-900 Feira de Santana, BA, Brazil
[b] Laboratório de Neuroquímica e Biologia Celular, Instituto de Ciências da Saúde, Universidade Federal da Bahia – UFBA, Av. Reitor Miguel Calmon s/n, Vale do Canela, 41100-100 Salvador, BA, Brazil
[c] Programa de Pós-Graduação em Desenvolvimento e Inovação Tecnológica em Medicamentos, Departamento de Ciências Molecular, Universidade Federal Rural de Pernambuco, Campus Dois Irmãos, 52171-900 Recife, PE, Brazil
[d] Laboratório de Ciências Químicas, Centro de Ciências e Tecnologia, Universidade Estadual do Norte Fluminense-Darcy Ribeiro, Av. Alberto Lamego, 2000-Parque Califórnia, 28013-602 Campos dos Goytacazes, RJ, Brazil
[e] PVE-FAPERJ/DEQUIM-ICE-Universidade Federal Rural do Rio de Janeiro (UFRRJ), CP 74541, 23894-374 Seropédica, RJ, Brazil
[f] LCQUI-CCT-Universidade Estadual do Norte Fluminense Darcy Ribeiro, 28013-600 Campos dos Goytacazes, RJ, Brazil

ARTICLE INFO

*Keywords:*
*Persea fulva*
Lauraceae
Alkene lactones
Molecular docking

ABSTRACT

The new alkene lactone, (3*E*)-5,6-dihydro-5-(hydroxymethyl)-3-docdecylidenefuran-3(4H)-one (**1**), named majoranolide B, and three alkene lactones known as majorenolide (**2**), majoranolide (**3**) and majorynolide (**4**) were obtained from the aerial parts of *Persea fulva* (Lauraceae). The structures were elucidated in light of extensive spectroscopic analysis, including 1D, 2D NMR ($^{1}$H, $^{13}$C, $^{1}$H-$^{1}$H-COSY, HMBC and HSQC) and HR-ESI-MS. These compounds were screened for their *in vitro* antiproliferative activity in rat C6 glioma and astrocyte cells using MTT assay and *in silico* by molecular docking against targets that play a central role in controlling glioma cell cycle progression. Majoranolide (**3**) is the most active compound with $IC_{50}$ 6.69 μM against C6 glioma cells, followed by the compounds **1** ($IC_{50}$ 9.06 μM), **2** ($IC_{50}$ 12.04 μM) and **4** ($IC_{50}$ 41.90 μM). The alkene lactones **1–3** exhibited lower toxicity in non-tumor cells when compared to glioma cells. Molecular docking results showed that majoranolide establishes hydrogen bonds with all targets through its α,β-unsaturated-γ-lactone moiety, whereas the long-chain alkyl group binds by means of several hydrophobic bonds. In the present study, it can be concluded from the anti-proliferative activity of isolates against C6 glioma cells that lactone constituents from *P. fulva* could have a great potential for the control of C6 glioma cells.

## 1. Introduction

Malignant gliomas are the most common and aggressive central nervous system tumors. Currently, the standard procedure for malignant gliomas consists of surgical resection followed by adjuvant chemotherapy [1,2]. Considering the lack of recent progress in the treatment, the development of new agents able to reactivate cell cycle or cell death programs is important for the new therapies focusing on malignant gliomas [3,4]. In this scenario, medicinal plant species and their secondary metabolites inhibit the progression and development of tumor cells [5].

The genus *Persea* of the family Lauraceae, comprising about 190 species, is widely distributed throughout Mesoamerica, South America and Southeastern Asia [6]. Previous phytochemical investigation of the genus *Persea* revealed the presence of terpenoids, flavonoids, lignans, alkaloids and steroids [7–16]. Alkene lactones also have been reported

*Abbreviations:* FAK, focal adhesion kinase; ERK1/2, Extracellular signal Regulated Kinase 1 and 2; S6K1, ribosomal protein S6 Kinase 1; COX-2, cyclooxygenase-2; MTT, 3-(4,5-dimethyl-2-thiazolyl)-2,5-diphenyl-2H-tetrazolium bromide

* Corresponding author.
*E-mail address:* branco@uefs.br (A. Branco).

https://doi.org/10.1016/j.bioorg.2019.02.023
Received 22 September 2018; Received in revised form 14 January 2019; Accepted 9 February 2019
Available online 14 February 2019
0045-2068/ 

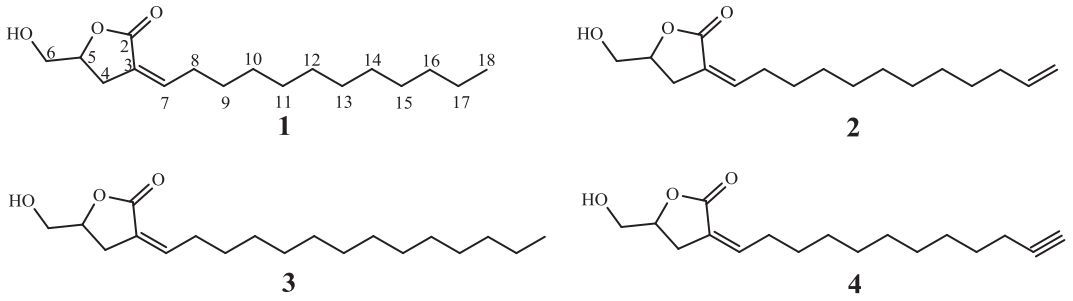


**Fig. 1.** Alkene Lactones (**1–4**) isolated from *P. fulva.* majoranolide B (**1**), majorenolide (**2**), majoranolide (**3**) and majorynolide (**4**).

in *Persea* species and have showed antitumoral and cytotoxic activities [17–20].

Due to the traditional medicinal importance of the genus and the few investigations with *Persea fulva* L.E. Koop., the aerial parts of this species were investigated, what yielded four alkene lactones (**1–4**) (Fig. 1). Herein, we described the isolation, structural elucidation and evaluation of the effects of these compounds on C6 glioma cell growth (*in vitro* and *in silico*).

## 2. Results and discussion

### 2.1. Isolation of alkene lactones

The leaves of *P. fulva* were collected from the Brazilian semiarid region and extracted with 80% ethanol. The EtOH extract was suspended in $H_2O$ and partitioned successively with hexane, EtOAc and *n*-ButOH. The EtOAc fraction was subjected to column chromatography to yield 15 fractions (Fr1-Fr15). The Fr 9-10 was subjected to purification by semi-preparative HPLC with DAD detection to afford the new natural compound (3*E*)-5,6-dihydro-5-(hydroxymethyl)-3-docdecylidenefuran-3(4H)-one, named majoranolide B (**1**), together with two other known alkene lactones: majorenolide (**2**) and majoranolide (**3**). Additionally, the Fr 8 was subjected to further column chromatography to afford another known alkene lactone, majorynolide (**4**). The elucidation of the compound structures was performed by 1D- and 2D-NMR techniques ($^1$H, $^{13}$C, HSQC, HMBC, $^1$H-$^1$H-COSY) (Table 1) as well as IR, HRESIMS and comparison with literature data.

Compound (**1**) was obtained as a green oil, whose molecular formula was determined to be $C_{17}H_{30}O_3$ by HRESIMS (*m/z* 283.2204, $[M+H]^+$) with a degree of unsaturation of 3. The $^{13}$C NMR and DEPT-135° spectra showed 17 carbons, including twelve methylenes at $\delta_C$ 26.3 (C-4), 63.2 (C-6), 29.6 (C-8), 27.8 (C-9), 29.4–29.0 (C-10 to C-15), 31.7 (C-16) and 22.3 (C-17), two quaternary carbons at $\delta_C$ 171.9 (C-2) and 126.8 (C-3), two methines at $\delta_C$ 78.2 (C-5) and 140.2 (C-7) and one methyl group at $\delta_C$ 13.0 (C-18).

One olefinic hydrogen was assigned the signal at $\delta$ 6.67 (m, H-C(7)) and three $CH_2$-group signals were observed $\delta$ 2.25 (q, $J$ = 7.4, $CH_2$(8)), 1.53 (qu, $J$ = 7.4, $CH_2$(9)), 1.30–1.45 (m, $CH_2$(10–17)). The presence of the signal at $\delta$ 0.92 (t, $J$ = 6.8 $CH_3$(18)) confirms the presence of a terminal methyl. One set of contiguous hydrogens was detected at $\delta$ 2.93 (m), 2.74 (m), for $CH_2$(4), 4.66 (m) for H-C(5) and 3.78 (dd, $J$ = 12.3, 3.2) and 3.60 (dd, $J$ = 12.3, 4.5) for $CH_2$(6). In addition, the α-alkylidene-γ-(hydroxymethyl)-γ-lactone moiety was deduced by the HMBC correlations of H-7 to C-2 and C-4; H-8 to C-2, C-3 and C-7 and H-4 to C-2, C-3, C-5, C-6 and C-7 (Fig. 2). The $CH_2$(4) hydrogens were also coupled to H-C(8) due to an allylic $^4J$-coupling, what suggested that **1** contains an α-alkylidene-γ-(hydroxymethyl)-γ-lactone moiety. Further spectral data (UV, HRESIMS, $^1$H and $^{13}$C NMR) confirmed the structure of **1** as (3*E*)-5,6-dihydro-5-(hydroxymethyl)-3-docdecylidenefuran-3(4H)-one, a new alkene lactone, named majoranolide B [17,19,21].

Compound **2** differs from **1** in the C-17 and C-18 terminal carbons, which in **2** show double bond signals and three additional olefinic hydrogens were assigned. Thus, according to the literature data, the structure of **2** was elucidated as majorenolide. The $^1$H and $^{13}$C NMR spectra for compound **3** were similar to those of **1**, except for the two additional carbons present in the side chain of **3**. Further spectral data confirmed the structure of **3** as majoranolide. The $^1$H and $^{13}$C NMR spectra of **4** were similar to those of majorenolide **2** and have the same α-alkylidene-γ-(hydroxymethyl)-γ-lactone moiety. The major difference was the presence of a terminal acetylene group. All spectral data confirmed the structure of **4** as majorynolide [17–19,21].

The High-Resolution Mass spectrometry multistage analysis (HR-ESI-MS/MS) of the alkene lactones **1–4** showed pseudo-molecular ion peak $[M+H]^+$ at *m/z* 283.2204, 281.2142, 311.2612 and 279.1966, respectively. $MS^2$ fragmentation of $[M+H]^+$ resulted in the formation of product ions from dehydration (**1a**, **2a**, **3a and 4a**), and neutral loss of formic acid (**1b**, **2b**, **3b** and **4b**), respectively. The Fig. S1 showed a proposal of fragmentation route of these compounds.

### 2.2. Antiproliferative activity

Unrestricted cell growth and resistance to cell death are typical hallmarks of tumor cells [22]. All isolated alkene lactones were evaluated for their effects on rat C6 glioma cell growth. The effect of alkene lactones on the metabolic activity of rat C6 glioma cells after 24 h of treatment was tested using the MTT reduction assay, which measures the dehydrogenase function in the mitochondrial metabolism. In order to calculate $IC_{50}$ values (concentration that causes 50% growth inhibition), the cells were incubated with increasing concentrations of the isolated compounds for 24 h.

When compared to control (DMSO 0.05%), it was observed that all the alkene lactones were cytotoxic ($p < 0.05$) to C6 cells, inducing significant decreases on mitochondrial activities (Fig. 3). Proliferation of C6 cells was significantly inhibited by alkene lactones in a concentration-dependent manner (Fig. 4), with more than 90% suppression. Majoranolide (**3**) is the most active compound with $IC_{50}$ 6.69 μM against C6 glioma cells, followed by the **1** ($IC_{50}$ 9.06 μM), **2** ($IC_{50}$ 12.04 μM) and **4** ($IC_{50}$ 41.90 μM) compounds.

C6 cells are still largely used *in vitro* and *in vivo* experimental models to develop new glioblastoma treatment strategies. Thus, some authors consider that results obtained from studies using C6 cells would be similar to responses observed in human glioblastomas [23].

Since the toxicity of the anticancer agents in the normal tissues reduces the possibilities of chemotherapy, the influence of the alkene lactones (1–4) on the viability of normal astrocytes was assessed. The results (Fig. 5) showed that alkene lactones **1–3** did not produce toxicity in astrocyte cells at concentrations greater than the $IC_{50}$ values for tumoral cells. Therefore, the results obtained for alkene lactones are promising in the search for new compounds with antitumor activity.

Majorenolide, majoranolide and majorynolide were isolated for the first time from the EtOH extract of the bark of *Persea major* and were all active in bioassays showing brine shrimp lethality inhibition of crown gall tumors on potato discs and cytotoxicity to human tumor cells (A-

**Table 1**
$^{1}H$ (500 MHz) and $^{13}C$ (125 MHz) NMR spectral data for alkene lactones (**1–4**) including results obtained by heteronuclear 2D shift-correlated HSQC ($^{1}J_{CH}$) and HMBC ($^{n}J_{CH}$, n = 2 and 3), in methanol-$d_4$ as solvent. Chemical shifts in δ (ppm), coupling constants (*J* in Hz, in parenthesis) and TMS as internal standard.

| | **1** | | **2** | | **3** | | **4** | |
|---|---|---|---|---|---|---|---|---|
| **C/H** | **δ ($^{13}C$)** | **δ ($^{1}H$)** | **δ ($^{13}C$)** | **δ ($^{1}H$)** | **δ ($^{13}C$)** | **δ ($^{1}H$)** | **δ ($^{13}C$)** | **δ ($^{1}H$)** |
| **C** | | | | | | | | |
| 2 | 171.9 | – | 171.9 | – | 171.9 | – | 171.9 | – |
| 3 | 126.8 | – | 126.8 | – | 126.8 | – | 126.8 | – |
| 17 | – | – | – | – | – | – | 82.8 | – |
| **CH** | | | | | | | | |
| 5 | 78.2 | 4.66 (m) | 78.2 | 4.66 (m) | 78.2 | 4.66 (m) | 78.2 | 4.65 (m) |
| 7 | 140.2 | 6.67 (m) | 140.2 | 6.67 (m) | 140.2 | 6.67 (m) | 140.2 | 6.67 (m) |
| 17 | – | – | 138.7 | 5.82 (m) | – | – | – | – |
| 18 | – | – | – | – | – | – | 67.9 | 2.17 (m) |
| **$CH_2$** | | | | | | | | |
| 4 | 26.3 | 2.93 (m), 2.74 (m) | 26.3 | 2.95 (m), 2.74 (m) | 26.3 | 2.94 (m), 2.74 (m) | 27.8 | 2.94 (m), 2.74 (m) |
| 6 | 63.2 | 3.78 (dd, 12.4, 3.3)<br>3.60 (dd, 12.4, 4.4) | 63.2 | 3.78 (dd, 12.3, 3.3)<br>3.60 (dd, 12.4, 4.5) | 63.2 | 3.78 (dd, 12.3, 3.3)<br>3.60 (dd, 12.4, 4.4) | 63.2 | 3.78 (dd, 12.3, 3.2)<br>3.59 (dd, 12.3, 4.6) |
| 8 | 29.6 | 2.25 (~q, 7.4) | 29.6 | 2.25 (q, 7.4) | 29.6 | 2.25 (~q, 7.4) | 29.6 | 1.50 (m) |
| 9 | 27.8 | 1.53 (qu, 7.4) | 27.8 | 1.52 (qu, 7.4) | 27.8 | 1.53 (qu, 7.4) | 28.2 | 1.54–1.25 |
| 10 | 29.4[a] | 1.45–1.30 | 29.2[b] | 1.40–1.30 | 29.4[c] | 1.40–1.30 | 29.1[d] | 1.54–1.25 |
| 11 | 29.4[a] | 1.45–1.30 | 29.1[b] | 1.40–1.30 | 29.4[c] | 1.40–1.30 | 29.0[d] | 1.54–1.25 |
| 12 | 29.2[a] | 1.45–1.30 | 29.1[b] | 1.40–1.30 | 29.4[c] | 1.40–1.30 | 29.0[d] | 1.54–1.25 |
| 13 | 29.1[a] | 1.45–1.30 | 29.0[b] | 1.40–1.30 | 29.4[c] | 1.40–1.30 | 28.7[d] | 1.54–1.25 |
| 14 | 29.0[a] | 1.45–1.30 | 28.8 | 1.40–1.30 | 29.2[c] | 1.40–1.30 | 28.3[d] | 1.54–1.25 |
| 15 | 29.0[a] | 1.45–1.30 | 28.7 | 1.40–1.30 | 29.1[c] | 1.40–1.30 | 28.2[d] | 1.54–1.25 |
| 16 | 31.7 | 1.45–1.30 | 33.4 | 2.06 (qu, 6.9) | 29.0[c] | 1.40–1.30 | 17.5 | 2.24 (m) |
| 17 | 22.3 | 1.45–1.30 | – | – | 29.0[c] | 1.40–1.30 | – | – |
| 18 | – | – | 113.3 | 4.98 (dq, 17.1, 1.6)<br>4.93 (dm, 10.1) | 31.7 | 1.40–1.30 | – | – |
| 19 | – | – | – | – | 22.0 | 1.40–1.30 | – | – |
| 20 | – | – | – | – | – | – | – | – |
| **$CH_3$** | – | – | – | – | – | – | | – |
| 18 | 13.0 | 0.92 (t, 6.8) | – | – | – | – | – | – |
| 19 | – | – | – | – | – | – | – | – |
| 20 | – | – | – | – | 13.0 | 0.92 (t, 6.8) | – | – |

Number of hydrogens bound to carbon atoms deduced by $^{13}C$-DEPTQ NMR spectra. Chemical shifts and coupling constants (*J*) obtained of 1D $^{1}H$ NMR spectra. Superimposed $^{1}H$ signals are described without multiplicity and chemical shifts deduced by HSQC, HMBC and $^{1}H$-$^{1}H$-COSY spectra.
[a,b,c,d] The δ ($^{13}C$) values with the same letter can be interchanged.

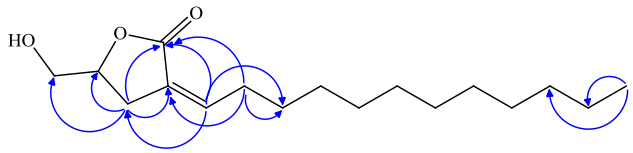


**Fig. 2.** HMBC correlations (blue arrows, from $^{1}H$ to $^{13}C$) of Majoranolide B (**1**).

549 lung carcinoma, MCF-7 breast carcinoma, HT-29 colon adenocarcinoma) [17,18]. Falodun et al. [20] described the isolation of one novel alkene lactone (4-hydroxy-5-methylene-3-undecyclidenedihydrofuran-2(3H)-one) from the root bark of *P. americana* and reported a stimulatory effect on non-tumorigenic MCF-12A cells regarding cell adhesion while tumorigenic MCF-7 cells detached continuously. These results corroborate with the abovementioned results for the alkene lactones isolated from *P. fulva*.

### 2.3. Molecular docking

A molecular docking approach can explain the interaction between molecules and proteins, which allows the characterization of the behavior of molecules at the binding site of target proteins [24]. In this study, we investigated pathways that play a central role in controlling glioma cell cycle progression. Four targets were selected, which are: Focal Adhesion Kinase (FAK) and Ribosomal protein S6 Kinase 1 (S6K1) because these targets are involved in multiple cellular functions such as cell proliferation, survival and metastasis [25–27]; Cyclooxygenase-2 (COX-2), because it has been reported to be overexpressed in several different tumor cells and hence has a crucial role in carcinogenesis and in the progress of disease [28]; and Extracellular signal Regulated Kinase 1 and 2 (ERK1/2) because they control the output of the MAPK pathway, which plays a central role in controlling mammalian cell cycle [24]. The crystallographic proteins used in the molecular docking studies are presented in the Table 2.

The efficiency and reproducibility of the docking protocol was checked by re-docking the native ligands in the active site of three enzymes. Docking success is observed when the pose is within 2 Å RMSD of the crystal ligand [29]. The RMSD of the predicted conformation was 0.95 Å for the S6K1, 0.18 Å for the FAK, 0.82 Å for the COX-2 and 0.36 Å for the ERK1/2 (Fig. S2). The results indicate that the DOCK 6.8 software was able to approach the structure experimentally determined.

Majoranolide (**3**) has shown the highest binding affinity with all targets in comparison to other alkene lactones tested (Table 3). For the FAK target, majoranolide (**3**) long-chain alkyl group forms hydrophobic interactions with the side chain of Leu567, Leu553, Ala452 and Glu506 residues, while hydrogen bonds were made from the oxygen of the majoranolide *α,β*-unsaturated-γ-lactone moiety and the N-terminal residue of the Asp564 and the oxygen atom of C-terminal residue of Glu500 (Fig. 6A). Literature data suggest that chiral and lactone ring compounds may have a strong interaction with this protein because lactone rings were responsible for hydrogen bonds with the binding pocket residues [26].

In the S6K1 docking, majoranolide forms hydrophobic interactions with the side chain of Leu13, Ala37, Val21, Lys39 and Lys157 and hydrogen bonds with the oxygen atom of the C-terminal residue of Lys-157 and the N-terminal residues of the Gly19 and Tyr18 (Fig. 6B). Thiyagarajan et al. [27] described that ligands form hydrogen bonds,

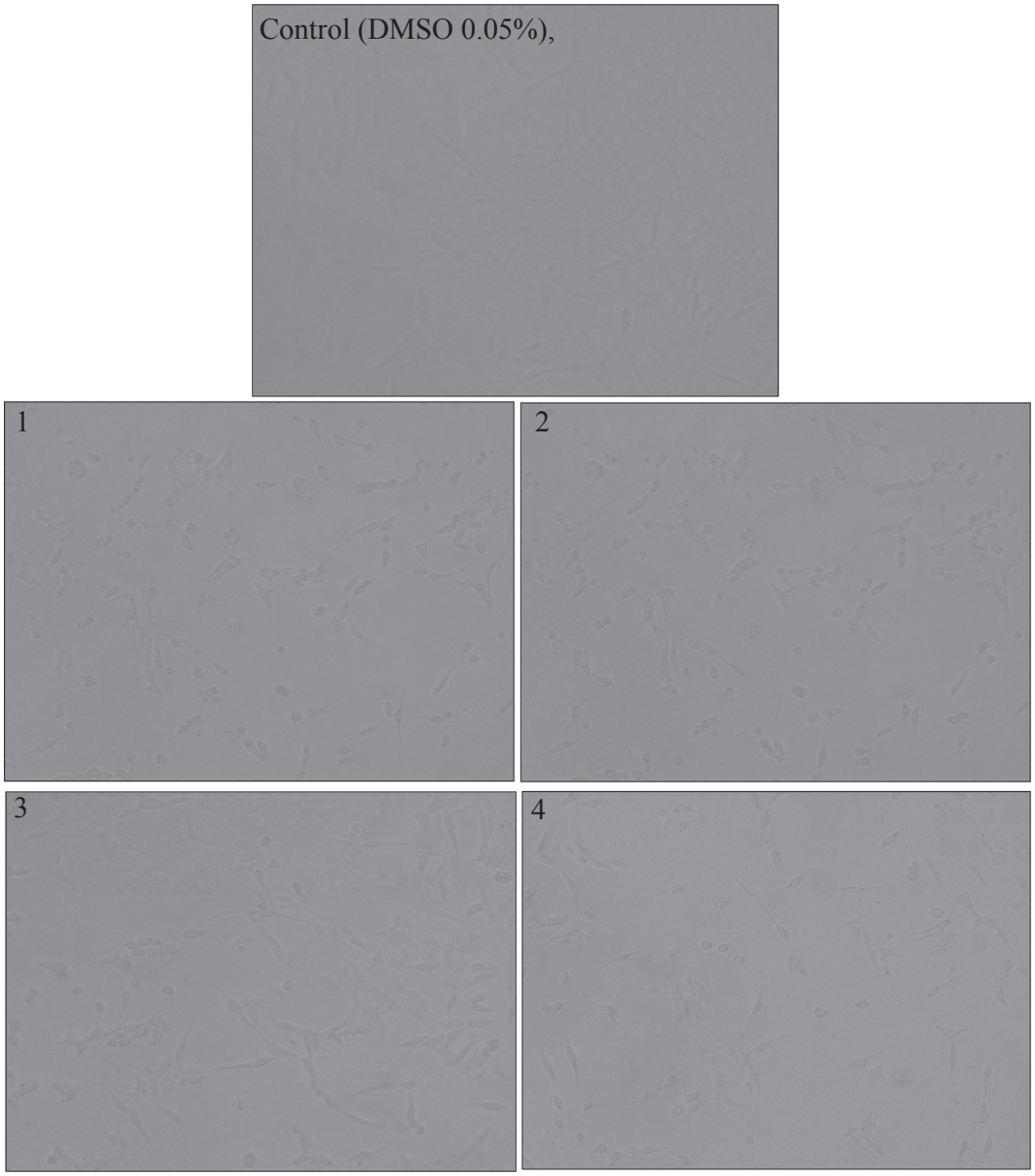


**Fig. 3.** Visual field of C6 cells treated with control (DMSO 0.05%), majoranolide B (**1**), majorenolide (**2**), majoranolide (**3**) and majorynolide (**4**) after 24 h after exposure with 10, 12, 7 and 40 μM, respectively.

Pi-cation and hydrophobic interactions with S1K6; these results confirm the abovementioned interactions between majoranolide and the S1K6 active site.

For COX-2, majoranolide (**3**) forms hydrophobic interactions with the side chain of Tyr84, Val85, Leu61, Tyr324, Leu500, Ala496 and Val318. The majoranolide (**3**) hydroxyl group forms a hydrogen bond with the oxygen atom of Met491 residue (Fig. 6C). Hydrophobic interactions account for the main interactions formed between ibuprofen (co-crystalized ligand) and the active site residues of COX-2 [30].

At last, for the ERK1/2 target, majoranolide (**3**) forms hydrophobic interactions with the benzene ring of Tyr36 and the side chain of Asp167, Val39, Ile31 and Leu156. A hydrogen bond was observed between the ligand hydroxyl groups and Met108, Lys114 and Glu109 (Fig. 6D).

For the all abovementioned interactions, majoranolide forms hydrogen bonds through its *α,β*-unsaturated-γ-lactone moiety, whereas the long-chain alkyl group coordinates with the target by means of several hydrophobic bonds. Hence, the bio-evaluation results indicated majoranolide as the compound with the lowest $IC_{50}$ and these results were further confirmed through docking studies. This compound showed the best affinity energy for all the targets.

## 3. Conclusion

One new and three already-known alkene lactones from *Persea fulva* were isolated and screened for their antitumor potential against C6 glioma cells. Among all compounds screened against C6 glioma cells, majoranolide (**3**) portrayed the potent activity followed by majoranolide B (**1**), majorenolide (**2**) and majorynolide (**4**). The molecular docking confirms majoranolide (**3**) as the most active and its interactions with the active site in four possible targets involved in antitumoral activity. Hence, from the anti-proliferative activity of isolates against C6 glioma cells, it can be concluded that lactone constituents from *P. fulva* could have a great potential for the control of C6 glioma cells.

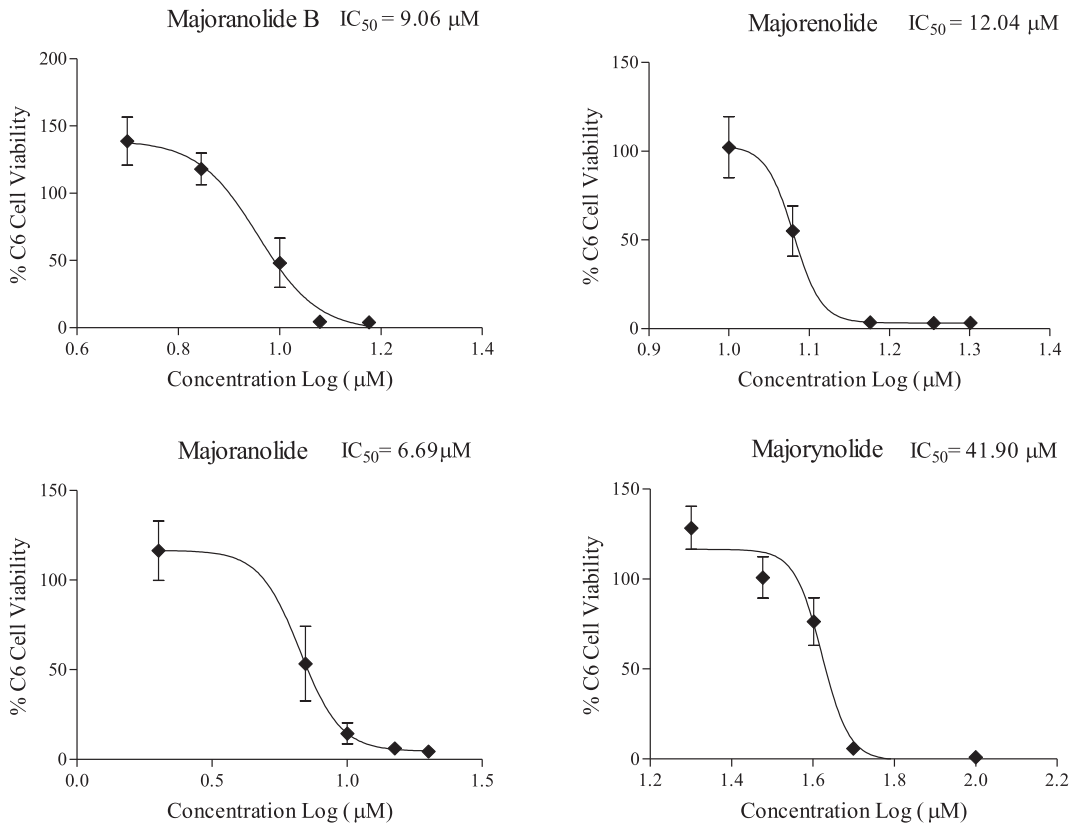


**Fig. 4.** C6 Cell viability was measured after 24 h using MTT activity assays. Error bars indicate means ± SD and $IC_{50}$ values were calculated using Graph Pad Prism 5. majoranolide B (**1**), majorenolide (**2**), majoranolide (**3**) and majorynolide (**4**).

## 4. Experimental section

### 4.1. General experimental procedures

Methanol was obtained from J.T. Baker (Deventer, The Netherlands). Milli-Q water was used for high-performance liquid chromatography (HPLC) analysis. HPLC was conducted using a Shimadzu Prominence Chromatograph, CMB-20A model (Shimadzu Corporation, Kyoto, Japan) equipped with a UV–vis detector (SPD-20A), column oven (CTO-20A), solvent pump (LC-20AD) and Luna Phenomenex C-18 column (Phenomenex, Aschaffenburg, Germany) (250 × 4.6 mm; 5 μm). The solvents $H_2O$ (A) and methanol (B) were used as the mobile phase in the following gradient elution: 0–4 min, 80–100% B; 4–10 min, 100% B; 10–12 min, 90% B. A semi-preparative HPLC system with DAD was used for the isolation of pure compounds and comprised a Luna Phenomenex C-18 column (Phenomenex, Aschaffenburg, Germany) (250 mm × 21.2 mm × 4 μm) with a 16-mL/min flow rate, with a binary gradient phase of $H_2O$ and methanol in the same conditions.

The XEVO-G2XSQTOF mass spectrometer (Waters, Manchester, UK) was connected to the ACQUITY UPLC system (Waters, Milford, MA, USA) via an electrospray ionization (ESI) interface. The analytical detector was a Waters Acquity PDA detector, which was set to a wavelength range of 200–400 nm. Chromatographic separation of compounds was performed on the ACQUITY UPLC with a conditioned autosampler at 4 °C, using an Acquity BEH C18 column (50 mm × 2.1 mm i.d., 1.7-μm particle size) (Waters, Milford, MA, USA). The column temperature was kept at 40 °C. The mobile phase consisting of 0.1% formic acid in water (solvent A) and methanol (solvent B) was pumped at a flow rate of 0.4 mL $min^{-1}$. The gradient elution program was as follows: 0–4 min, 80–100% B; 4–10 min, 100% B; 10–11 min, 90% B. The injection volume was 10 μL. MS analysis was performed on a Xevo G2 QTOF (Waters MS Technologies, Manchester, UK), a quadrupole time-of-flight tandem mass spectrometer coupled with an electrospray ionization source in positive ion mode. The scan range was from 50 to 1200 *m/z* for data acquisition. Source conditions were as follows: capillary voltage, 2.0 kV; sample cone, source temperature, 100 °C; desolvation temperature 250 °C; cone gas flow rate 20 L $h^{-1}$; desolvation gas ($N_2$) flow rate 600 L $h^{-1}$. All analyses were performed using the lockspray (10 μL $min^{-1}$), which ensured accuracy and reproducibility.

$^1H$ (500 MHz) and $^{13}C$ (125 MHz) NMR data were obtained on a Bruker Advance II 9.4 T instrument (Centro de Ciências e Tecnologia, UENF) using methanol-$d_4$ as solvent. Data are reported as follows: chemical shift ($\delta$), multiplicity (s = singlet, d = doublet, t = triplet, q = quartet, br = broad, m = multiplet), integration, coupling constants ($J$ = Hz) and assignment. Measure of IR data was on Shimadzu IRAffinity-1.

### 4.2. Plant material

Leaves of *P. fulva* (1050 g) were collected in Rio de Contas (Latitude 13°22′26.9″S; Longitude 41°53′27.5″W), Bahia, Brazil, in August 2012. The plant material was identified by PhD Francisco Haroldo Feitosa do Nascimento (State University of Feira de Santana). A voucher specimen (n. 201.418) was deposited in the Herbarium of State University of Feira de Santana.

### 4.3. Extraction and isolation

Leaves of *P. fulva* (1050 g) were ground into a powder, then extracted with EtOH-$H_2O$ (3000 mL, 80:20 v/v, 5 days each time) at room temperature for three times. After removal of the combined solvents, a crude extract (193 g) was obtained. The crude extract was suspended in $H_2O$ and partitioned with hexane, EtOAc and *n*-ButOH (each 900 mL) in succession. The resulting three fractions were evaporated in vacuum

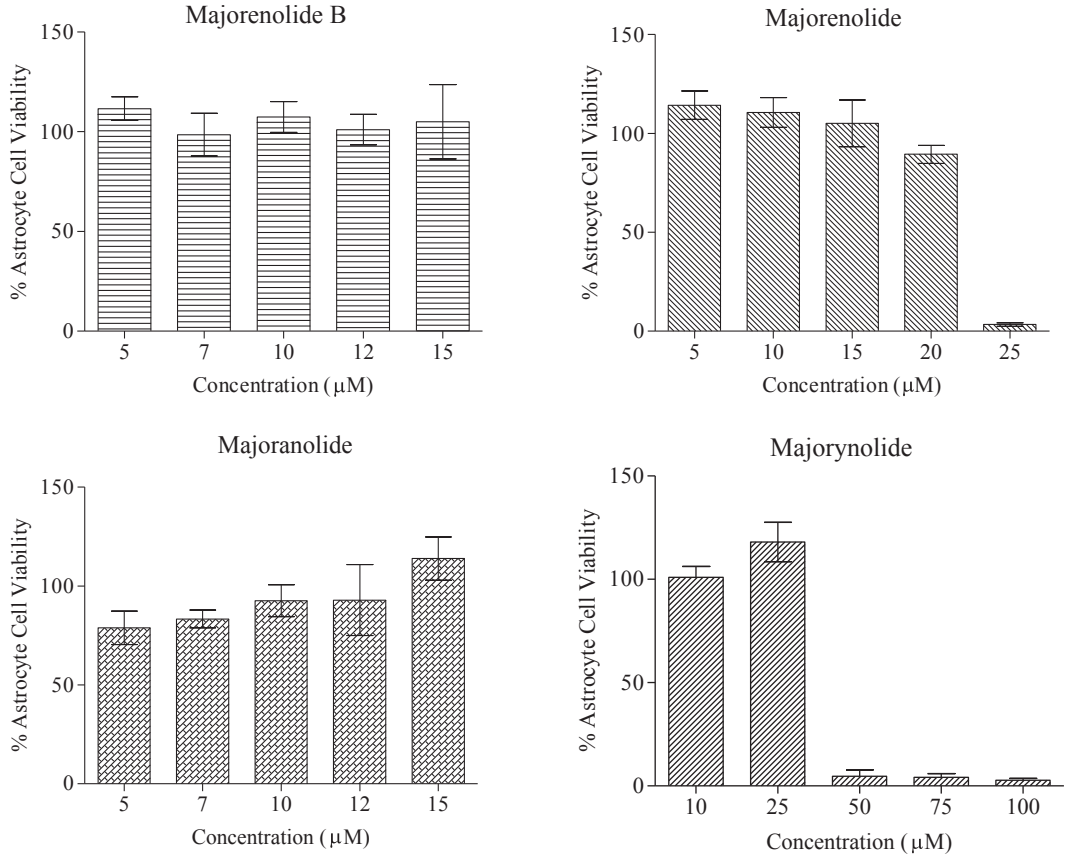


**Fig. 5.** Astrocyte cell viability was measured after 24 h using MTT activity assays. Error bars indicate means ± SD of compunds majoranolide B (**1**), majorenolide (**2**), majoranolide (**3**) and majorynolide (**4**).

drying to yield hexane (7 g), EtOAc (62 g) and *n*-ButOH (34 g). Subsequently, the EtOAc fraction was subjected to silica gel CC using as mobile phase, solvents of increasing polarity (hexane, EtOAc, MeOH and $H_2O$) to yield subfractions 1–15.

The fractions 9–10 (2.9 g) were submitted to semi-preparative HPLC-DAD analysis for the isolation of compounds **1** ($t_R$. 11.5 min; 146 mg, purity > 78% by HPLC), **2** ($t_R$. 10.8 min; 1900 mg, purity > 95% by HPLC), **3** ($t_R$. 12.7 min; 223 mg, purity > 95% by HPLC). The fraction 8 was purified by silica gel column chromatography (hexane: EtOAc, 9:1/7:3) to yield compound **4** (35 mg, purity > 95% by HPLC).

### 4.4. Spectral data

**Majoranolide B (1)**: Colorless crystals (146 mg); IR (KBr) $\lambda_{max}$: 3441, 2924, 2853, 1751, 1678, 1643, 1464 and 1213 $cm^{-1}$; $^1H$ NMR (methanol-$d_4$, 500 MHz) and $^{13}C$ NMR (methanol-$d_4$, 125 MHz) spectroscopic data: see Table 1. HR-ESI-MS: *m/z* 283.2290 $[M+H]^+$ (calcd. for $C_{17}H_{32}O_3$ $[M+H]^+$: 283.2267).

**Majorenolide (2)**: Green oil (1900 mg); IR (KBr) $\lambda_{max}$: 3397, 2926, 2855, 1751, 1641, 1462, 1439 and 1200 $cm^{-1}$; $^1H$ NMR (methanol-$d_4$, 500 MHz) and $^{13}C$ NMR (methanol-$d_4$, 125 MHz) spectroscopic data: see Table 1. HR-ESI-MS: *m/z* 281.2119 $[M+H]^+$ (calcd. for $C_{17}H_{30}O_3$ $[M+H]^+$: 281.2111).

**Majoranolide (3)**: Colorless crystals (223 mg); IR (KBr) $\lambda_{max}$: 3736, 3610, 2920, 2850, 1743, 1678, 1523 and 1211 $cm^{-1}$; $^1H$ NMR (methanol-$d_4$, 500 MHz) and $^{13}C$ NMR (methanol-$d_4$, 125 MHz) spectroscopic data: see Table 1. HR-ESI-MS: *m/z* 311.2599 $[M+H]^+$ (calcd. for $C_{19}H_{36}O_3$ $[M+H]^+$: 311.2580).

**Majorynolide (4)**: Colorless oil (35 mg); IR (KBr) $\lambda_{max}$: 3443, 3308, 2928, 2854, 1745, 1680, 1643, 1462 and 1205 $cm^{-1}$; $^1H$ NMR (methanol-$d_4$, 500 MHz) and $^{13}C$ NMR (methanol-$d_4$, 125 MHz) spectroscopic data: see Table 1. HR-ESI-MS: *m/z* 279.1966 $[M+H]^+$ (calcd. for $C_{17}H_{28}O_3$ $[M+H]^+$: 279.1954).

### 4.5. Antiproliferative activity

#### 4.5.1. Cell cultures

Rat C6 glioma cells were cultured until confluence in 10-mm polystyrene plates (TPP, Trasadingen, Switzerland), trypsinized and replated on 40-mm ($1.5 \times 10^5$ cells/plate) or in 96-well ($5 \times 10^3$ cells/$cm^2$) polystyrene culture dishes (TPP). These cultures were cultured in Dulbecco's modified Eagle's medium (DMEM; Cultilab, Campinas, Brazil) supplemented with 100 UI/mL penicillin G, 100 mg/mL streptomycin, 7 mmol/L glucose, 2 mmol/L L-glutamine, 0.011 g/L pyruvic acid and 10% fetal calf serum and maintained in a humidified atmosphere composed of 95% air and 5% $CO_2$ at 37 °C.

Astrocyte cells were obtained from the cortex of Wistar newborn rats (0–2 days old) from the Animal Facility of the Federal University of Bahia (Salvador, Brazil) and performed according to Brazilian guidelines for production, maintenance and use of animals for teaching activities and scientific research and the local Ethical Committee for Animal Experimentation, protocol number (0272012, ICS - UFBA). In brief, after decapitation, the forebrains of newborn Wistar rats were dissociated mechanically and resuspended in DMEM supplemented with 10% Fetal Bovine Serum (FBS), 10% Serum equine (HS), 4 mM L-glutamine, 100 U/mL penicillin and 100 μg/mL streptomycin. The cells were cultured on poly-D-lysine (25 μg/mL) -coated flasks. Upon reaching confluence (7–10 days), adherent microglial cells were harvested by shaking at 165 rpm at 37 °C for 3 h. After agitation to remove microglia, the cultures enriched in astrocytes will be kept in the oven for 48 h. After that period, they were trypsinized and seeded in 96-well plates at a density of $3 \times 10^4/cm^2$ and experiments were performed

**Table 2**
Molecular targets used in docking studies.

| Target | Ligand | GridScore Energy (kcal mol$^{-1}$) | PDB ID | Resolution (Å) | Reference |
|---|---|---|---|---|---|
| Focal adhesion kinase (FAK) | 2-({5-chloro-2-[(2-methoxy-4-morpholin-4-ylphenyl)amino]pyrimidin-4-yl}amino)-*n*-methylbenzamide | − 57.59 | 2JKK | 2.0 | [25] |
| Extracellular signal Regulated Kinase 1 and 2 (ERK1/2) | 5-(2-methoxyethyl)-2-[2-(oxan-4-ylamino)pyrimidin-4-yl]-6,7-dihydro-1-(H)-pyrrolo[3,2-c]pyridin-4-one | − 78.99 | 5NHH | 1.94 | [24] |
| Cyclooxygenase-2 (COX-2) | Ibuprofen | − 53.63 | 4PH9 | 1.81 | [30] |
| Ribosomal protein S6 Kinase 1 (S6K1) | 2-{[4-(5-ethylpyrimidin-4-yl)piperazin-1-yl]methyl}-5-(trifluoromethyl)-1H-benzimidazole | − 64.87 | 4L3J | 2.1 | [41] |

**Table 3**
Docking results for the isolated compounds (**1–4**) against each molecular targets.

| Compounds | Targets (GridScore – kcal mol$^{-1}$) | | | |
|---|---|---|---|---|
| | FAK | S6K1 | COX-2 | ERK1/2 |
| Majoranolide B (**1**) | − 40.22 | − 61.66 | − 56.89 | − 61.99 |
| Majorenolide (**2**) | − 39.72 | − 60.98 | − 56.37 | − 62.41 |
| Majoranolide (**3**) | − 42.41 | − 65.41 | − 62.10 | − 65.40 |
| Majorynolide (**4**) | − 39.35 | − 60.55 | − 55.53 | − 62.80 |

after 24 h. In all cases, the cells were cultured at 37 °C in 5% $CO_2$.

#### 4.5.2. Treatments and cell viability evaluation

The inhibition ratio reflecting the cytotoxicity of the compounds was assessed through an MTT assay [31]. Confluent cancer cells cultured in 96-well plates (TPP) (1x10$^4$ cells/mL, 100 µL each well) were exposed to compounds **1–4** (1–50 µM) for 24 h. Two hours before the end of the exposure time, the culture medium was replaced by a solution of MTT diluted in DMEM (5 mg/mL) and then the plate was incubated for 2 h in a humidified atmosphere with 5% $CO_2$ at 37 °C. Thereafter, cells were lysed with 20% (w/v) sodium dodecyl sulfate (SDS), 50% (v/v) acetic acid and 2.5% (v/v) 1 mol/L HCl. The plates were kept overnight at 37 °C to allow the formazan crystals to dissolve. The cell cytotoxicity was quantified by measuring the conversion of yellow MTT into purple MTT formazan by mitochondrial dehydrogenases of living cells. The optical density of each sample was measured at 540 nm using a Bio-Rad 550 PLUS Spectrophotometer (Bio-Rad, Santo Amaro, Brazil). Control cells were treated with the same volume of DMSO (0.1%) diluted in DMEM, which was used as a vehicle for compounds **1–4**. Three independent experiments were conducted and eight replicate wells were used for each experimental condition.

#### 4.5.3. Statistical analysis

Results were expressed as mean ± standard deviation and analyzed with ANOVA followed by Tukeý́s test. Values of $P < 0.05$ were considered as significant. The $IC_{50}$ (inhibitory concentration 50%) of the compounds was calculated through nonlinear regression analysis. All statistical analyses were performed using the Graphprism statistical program (version 5.0, GraphPad Software Inc., La Jolla, California, USA).

### 4.6. Molecular docking

The 2D chemical structure of the alkene lactones was generated on the Marvin Sketch 6.0.1 software, 2013, ChemAxon (http://www.chemaxon.com) and the 2D coordinates were converted into the 3D format with the help of the SYBYL-X 2.0 software (Tripos Associates, St. Louis, MO, USA) [32]. The Gasteiger-Huckel charges were calculated with the FF12SB method [33], as available in Chimera 1.10.1.

The molecular targets were taken to the Protein Data Bank (PDB) and the selection was based on the best resolution value (Table 2). The 3D structure selected is shown in Table 2. The co-crystalized ligands were utilized to locate the active site in the molecular targets. The molecular targets were prepared through the DockPrep module on the Chimera 1.10.1 software [34] for the removal of water molecules and the addition of polar hydrogens to optimize the hydrogen bonds. The ions and cofactors were maintained for molecular targets (4PH9 and 4L3J).

The molecular docking was performed on the DOCK 6.8 software [35]. Initially, the solvent accessible surface of the molecular targets was calculated using the DMS software, without hydrogen atoms, using a probe radius of 1.4 Å [36]. Using the SPHGEN and SPHERE_SELECTOR pieces of software, the docking space was defined using the co-crystalized ligand for each molecular target. The molecular properties

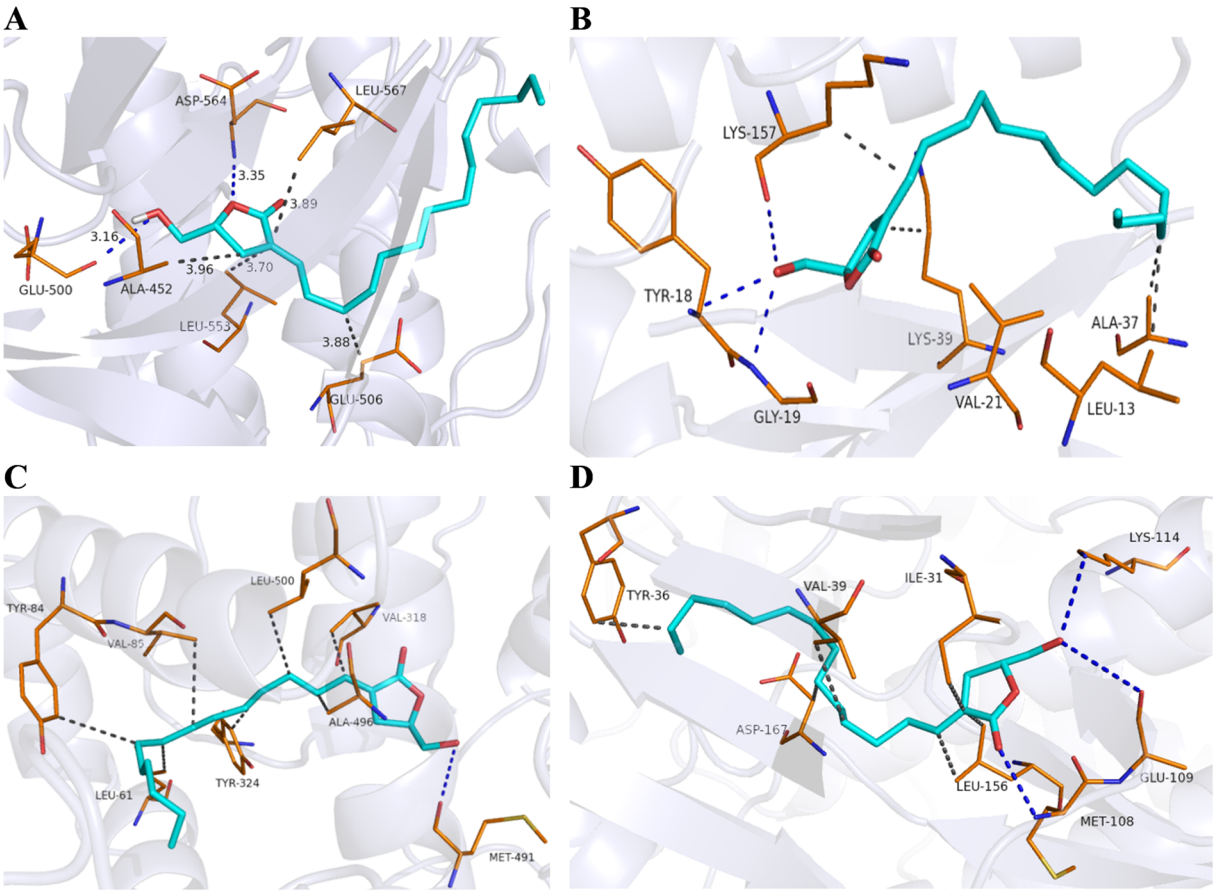


**Fig. 6.** Docking results for FAK (A) S6K1 (B), COX-2 (C) and ERK1/2 (D). Carbons are represented in cyan or orange, nitrogen in blue and oxygens in red. Blue dashed line: hydrogen bond; Grey dashed line: hydrophobic interaction.

(potential attraction and repulsion, solvation effects and steric contacts) for the region were calculated using the GRID software in default setting [37,38]. The molecular docking was performed using the GridScore scoring function [39]. A redocking process was performed to verify the accuracy of the docking method to reproduce the crystallographic orientation of the complexed ligands to the selected targets. The results were analyzed using Root-Mean-Square Deviation (RMSD) calculated on the DOCK6.8 software. Next, a set of alkene lactones (**1–4**) were docked against all the proteins.

The analysis of the intermolecular interactions for the top-ranked molecule for each target was performed in the Protein-Ligand Interaction Profiler software [40] and the interaction maps were designed on PyMOL v0.99.

## Acknowledgments

The authors are grateful to Coordenação de Aperfeiçoamento de Pessoal de Nível Superior (CAPES), Fundação de Amparo à Pesquisa do Estado da Bahia (FAPESB), Fundação de Amparo à Pesquisa do Estado de Pernambuco (FACEPE) and Conselho Nacional de Desenvolvimento Científico e Tecnológico (CNPq) for the grants and fellowship. We also thank teacher Abilio Borghi for the grammar review of the manuscript.

## Appendix A. Supplementary material

Supplementary data to this article can be found online at https://doi.org/10.1016/j.bioorg.2019.02.023.

## References

[1] L. Yin, H. Li, W. Liu, Z. Yao, Z. Cheng, H. Zhang, H. Zou, A highly potent CDK4/6 inhibitor was rationally designed to overcome blood brain barrier in gliobastoma therapy, Eur. J. Med. Chem. 144 (2018) 1–28.
[2] S. Roy, D. Lahiri, T. Maji, J. Biswas, Recurrent glioblastoma: where we stand, South Asian J. Cancer 4 (2015) 163–173.
[3] M. Zielińska-Przyjemska, M. Kaczmarek, V. Krajka-Kuźniak, M. Łuczak, W. Baer-Dubowska, The effect of resveratrol, its naturally occurring derivatives and tannic acid on the induction of cell cycle arrest and apoptosis in rat C6 and human T98G glioma cell lines, Toxicol. In Vitro 43 (2017) 69–75.
[4] Y. Dagistan, I. Karaca, E.R. Bozkurt, E. Ozar, K. Yagmurlu, A. Toklu, A. Bilir, Combination hyperbaric oxygen and temozolomide therapy in C6 rat glioma model, Acta Cir. Bras. 27 (2012) 383–387.
[5] J. Iqbal, B.A. Abbasi, T. Mahmood, S. Kanwal, B. Ali, S.A. Shah, A.T. Khalil, Plant-derived anticancer agents: a green anticancer approach, Asian Pac. J. Trop. Biomed. 7 (2017) 1129–1150.
[6] R. Scora, B. Bergh, The origin and taxonomy of avocado (*Persea americana* Mill. Lauraceae), Acta Hortic. 275 (1990) 387–394.
[7] A.K. Kruthiventi, N. Krishnaswamy, Constituents of the flowers of *Persea gratíssima*, Fitoterapia 71 (2000) 94–96.
[8] H. Ding, Y.-W. Chin, A.D. Kinghorn, S.M. D'Ambrosio, Chemopreventive characteristics of avocado fruit, Semin. Cancer Biol. 17 (2007) 386–394.
[9] B.E. Wofford, The systematic significance of flavonoids in *Persea* of the Southeastern United States, Biochem. Syst. Ecol. 2 (1974) 89–91.
[10] A. Gonzalez-Coloma, R. Cabrera, P. Castarera, C. Gutierrez, B.M. Fraga, Insecticidal activity and diterpene content of *Persea indica*, Phytochemistry 31 (1992) 1549–1552.
[11] I.-L. Tsai, C.-F. Hsieh, C.-Y. Duh, I.-S. Chen, Cytotoxic neolignans from *Persea obovatifolia*, Phytochemistry 43 (1996) 1261–1263.
[12] A.N.L. Batista, J.M. Batista Junior, S.N. Lopez, M. Furlan, A.J. Cavalheiro, D.H.S. Silva, V.S. Bolzani, S.M. Nunomura, M. Yoshida, Aromatic compounds from three Brazilian Lauraceae species, Quim. Nova 33 (2010) 321–323.
[13] C.-C. Wang, C.-S. Kuoh, T.-S. Wu, Constituents of *Persea japonica*, J. Nat. Prod. 59 (1996) 409–411.
[14] S. Sepulveda-Boza, S. Delhvi, B.K. Cassels, An aryltetralin lignan from *Persea lingue*, Phytochemistry 29 (1990) 2357–2358.
[15] N. Prasitpan, T. Patharakorn, P. Sutthivaiyakit, P. Denrungruang, Lignans from the bark of *Persea kurzii* Kosterm, Nat. Sci. 30 (1996) 493–505.

[16] M.R. Ramos, G. Jerz, S. Villanueva, F. Lopez-Dellamary, R. Waibel, P. Winterhalter, Two glucosylated abscisic acid derivates from avocado seeds (*Persea americana* Mill. Lauraceae cv. Hass), Phytochemistry 65 (2004) 955–962.
[17] W. Ma, J.E. Anderson, C. Chang, D.L. Smith, J.L. Mclaughlin, Majorenolide and majorynolide: a new pair of cytotoxic and pesticidal alkene alkyne & lactones from *Persea major*, J. Nat. Prod. 52 (1989) 1263–1266.
[18] W. Ma, J.E. Anderson, C. Chang, D.L. Smith, J.L. Mclaughlin, Majoranolide: a lactone from *Persea major*, Phytochemistry 29 (1990) 2698–2699.
[19] S.Y. Chang, M.J. Cheng, C.F. Peng, H.S. Chang, I.S. Chen, Antimycobacterial butanolides from the root of Lindera akoensis, Chem. Biodivers. 5 (2008) 2690–2698.
[20] A. Falodun, N. Engel, U. Kragl, B. Nebe, P. Langer, Novel anticancer alkene lactone from *Persea americana*, Pharm. Biol. 51 (2013) 700–706.
[21] B.M. Fraga, D. Terrero, Alkene lactones and avocadofurans from *Persea indica*: a revision of the structure majorenolide of and related lactones, Phytochemistry 41 (1996) 229–232.
[22] D. Hanahan, R.A. Weinberg, Hallmarks of cancer: the next generation, Cell 144 (2011) 646–674.
[23] R.S. Ignarro, G. Facchini, D.R. Melo, K.J. Pelizzaro-Rocha, C.V. Ferreira, R.F. Castilho, F. Rogerio, Characteristics of sulfasalazine-induced cytotoxicity in C6 rat glioma cells, Neurosci. Lett. 638 (2017) 189–195.
[24] R.A. Ward, P. Bethel, C. Cook, E. Davies, J.E. Debreczeni, G. Fairley, L. Feron, V. Flemington, M.A. Graham, R. Greenwood, N. Griffin, L. Hanson, P. Hopcroft, T.D. Howard, J. Hudson, M. James, C.D. Jones, C.R. Jones, S. Lamont, R. Lewis, N. Lindsay, K. Roberts, I. Simpson, S. St-Gallay, S. Swallow, J. Tang, M. Tonge, Z. Wang, B. Zhai, Structure-guided discovery of potent and selective inhibitors of ERK1/2 from a modestly active and promiscuous chemical start point, J. Med. Chem. 60 (2017) 3438–3450.
[25] D. Lietha, M.J. Eck, Crystal structures of the FAK kinase in complex with TAE226 and related bis-anilino pyrimidine inhibitors reveal a helical Dfg conformation, Plos One 3 (2008) 1–7.
[26] V. Thiyagarajan, S.H. Lin, Y.C. Chia, C.F. Weng, A novel inhibitor, 16-hydroxy-cleroda-3,13-dien-16,15-olide, blocks the autophosphorylation site of focal adhesion kinase (Y397) by molecular docking, Biochim. Biophys. Acta 2013 (1830) 4091–4101.
[27] V. Thiyagarajan, S.H. Lin, Y.C. Chang, C.F. Weng, Identification of novel FAK and S6K1 dual inhibitors from natural compounds via ADMET screening and molecular docking, Biomed. Pharmacother. 80 (2016) 52–62.
[28] B. Sever, M.D. Altıntop, G. Kus, M. Ozkurt, A. Ozdemir, Z.A. Kaplancıklı, Indomethacin based new triazolothiadiazine derivatives: synthesis, evaluation of their anticancer effects on T98 human glioma cell line related to COX-2 inhibition and docking studies, Eur. J. Med. Chem. 113 (2016) 179–186.
[29] S.R. Brozell, S. Mukherjee, T.E. Balius, D.R. Roe, D.A. Case, R.C. Rizzo, Evaluation of DOCK 6 as a pose generation and database enrichment tool, J. Comput. Aided. Mol. Des. 26 (2012) 749–773.
[30] B.J. Orlando, M.J. Lucido, M.G. Malkowski, The structure of ibuprofen bound to cyclooxygenase-2, J. Struct. Biol. 189 (2015) 62–66.
[31] Q.-X. Yue, Z.-W. Cao, S.-H. Guan, X.-H. Liu, L. Tao, W.-Y. Wu, Y.-X. Li, P.-Y. Yang, X. Liu, D.-A. Guo, Proteomics characterization of the cytotoxicity mechanism of ganoderic acid D and computer-automated estimation of the possible drug target, Mol. Cell. Proteom. 7 (2008) 949–961.
[32] Tripos International, 2012. Sybyl-X 2.0, Tripos International, St. Louis, MO, USA.
[33] J. Gasteiger, M. Marsili, Iterative partial equalization of orbital electronegativity – a rapid access to atomic charges, Tetrahedron 36 (1980) 3219–3228.
[34] E.F. Pettersen, T.D. Goddard, C.C. Huang, G. Couch, D.M. Greenblatt, E.C. Meng, T.E. Ferrin, UCSF Chimera – a visualization system for exploratory research and analysis, J. Comput. Chem. 25 (2004) 1605–1612.
[35] W.J. Allen, T.E. Balius, S. Mukherjee, S.R. Brozell, D.T. Moustakas, P.T. Lang, L. Jiang, T.D. McGee Jr., S. Mukherjee, Y. Zhou, R. Rizzo, D. Case, B. Shoichet, I. Kuntz, DOCK 6: impact of new features and current docking performance, J. Comput. Chem. 36 (2015) 1132–1156.
[36] T.E. Ferrin, C.C. Huang, L.E. Jarvis, R. Langridge, The Midas display system, J. Mol. Graf. 6 (1988) 13–27.
[37] I.D. Kuntz, J.M. Blaney, S.J. Oatley, R. Langridge, T.E. Ferrin, A geometric approach to macromolecule–ligand interactions, J. Mol. Biol. 161 (1982) 269–288.
[38] B.K. Shoichet, I.D. Kuntz, D.L. Bodian, Molecular docking using shape descriptors, J. Comput. Chem. 13 (1992) 380–397.
[39] E.C. Meng, B.K. Shoichet, I.D. Kuntz, Automated docking with grid-based energy evaluation, J. Comp. Chem. 13 (1992) 505–524.
[40] S. Salentin, S. Schreiber, V.J. Haupt, M.F. Adasme, M. Schroeder, PLIP: fully automated protein-ligand interaction profiler, Nucl. Acids Res. 43 (2015) W443–W447.
[41] J. Wang, C. Zhong, F. Wang, F. Qu, J. Ding, Crystal structures of S6K1 provide insights into the regulation mechanism of S6K1 by the hydrophobic motif, Biochem. J. 454 (2013) 39–47.